Optical coherence of ^{166}Er:^{7}LiYF$_4$ crystal below 1 Kelvin

N. Kukharchyk,[1] D. Sholokhov,[1] S. L. Korableva,[2] A. A. Kalachev,[2,3] and P. A. Bushev[1]

[1]*Experimentalphysik, Universität des Saarlandes, D-66123 Saarbrücken, Germany*
[2]*Kazan Federal University, 420008 Kazan, Russian Federation*
[3]*Kazan Institute of Physics and Technology, 420029 Kazan, Russian Federation*

(Dated: March 23, 2017)

We explore spin dynamics of isotopically purified ^{166}Er:^{7}LiYF$_4$ crystal below 1 Kelvin and at weak magnetic fields <0.3 T. Crystals grown in our lab demonstrate record-narrow inhomogeneous optical broadening down to 16 MHz. Solid state atomic ensembles with such narrow linewidths are very attractive for the implementation of off-resonant Raman quantum memory and for the interfacing of superconducting quantum circuits and telecom C-band optical photons. Both applications require low magnetic field of ~ 10 mT. However, at conventional experimental temperatures $T > 1.5$ K and time scales of μs, spin coherence of Er:LYF crystal appears only at magnetic fields above 1 Tesla. In the present work, we demonstrate spin coherence of Er:LYF crystals at the field range compatible with ZEFOZ transitions of ^{167}Er isotope and with working conditions of superconducting quantum circuits.

arXiv:1703.07621v1 [physics.optics] 22 Mar 2017

Rare-earth (RE) doped solids represent today one of the widely exploited materials for the modern laser and telecommunication industry. Yet, recently, they have raised a strong interest in the field of quantum information storage, signal processing and communication [1]. The crucial figure of merit which characterizes a value of a material for its application in quantum memory is its optical or spin coherence time. Due to the long coherence time of optically addressable spin states [2, 3], RE doped crystals are especially attractive as memory elements in quantum repeaters [4]. In order to attain long coherence time, high magnetic field up to 7 T and low temperatures of 1.5 K are required. By following this prescription the longest optical coherence time of 4.4 ms among solid state systems has been demonstrated for 0.001% Er^{3+}:Y_2SiO_5 (Er:YSO) [5]. Also, in the very recent experiments M. Rančić et al. demonstrated optically addressable hyperfine states of ^{167}Er:YSO with coherence time of 1.3 second [3].

Even longer spin coherence time of 6 hours was attained for non-Kramers Pr^{3+} ion by using Zero First Order Zeeman (ZEFOZ) shift technique [2]. The basic idea of such technique is to map quantum state of incoming optical photon into long-lived hyperfine spin state which is insensitive to the magnetic field fluctuations [6]. Kramers ions also reveal ZEFOZ transitions at weak magnetic fields of $\sim 0.01-0.1$ T. However, at weak fields and at conventional temperatures of $T > 1.5$ K, spin coherence time of hyperfine and Zeeman lifetimes is shortened by spin-lattice relaxation process and by interaction with electronic spins of RE-ions [5, 7, 8]. In order to diminish the role of such decoherence processes we propose to cool down RE-doped crystals to ultra-low temperatures ($T < 1$ K). At sub-Kelvin temperatures the substantial polarization of electronic spin bath can be attained already at ~ 0.1 T [9] and spin relaxation time is longer by orders of magnitude [10, 11]. Following up our proposal we investigate optical coherence of isotopically purified $^{166}Er^{3+}$:^{7}LiYF$_4$ (Er:LYF) crystal at sub-Kelvin temperatures and at the magnetic field range of $0-0.3$ T. Since optical transition of erbium ions occur between Zeeman sub-levels in magnetic field, its coherence is strongly influenced by magnetic fluctuations of electron and nuclear spin baths and in our optical experiment we also study quantum spin dynamics of erbium ions in completely new regime.

Isotopically purified LYF crystals are well known for their ultra-narrow optical inhomogeneous broadening $\sim$10 MHz limited by nuclear spin fields [12, 13]. Narrow optical transitions are very attractive for the solid-state implementation of quantum memory based on off-resonant Raman protocols [14, 15], and therefore today Er:LYF is again in the focus of the increasing interest [16, 17]. In contrast to Er:YSO, Er:LYF crystal requires quite high magnetic field $B > 1$ T and temperatures $T \sim 1.5$ K for the establishing of spin coherence at $\sim \mu$s timescale [18, 19]. However, ZEFOZ points of ^{167}Er hyperfine transitions occurs at weak fields of ~ 10 mT, therefore much lower temperatures are necessary for the operation of Raman quantum memory based on LYF crystals.

The single crystal $^{166}Er^{3+}$:^{7}LiYF$_4$ (0,005 at%) was grown in our lab by using Bridgman-Stockbarger method in graphite crucibles in argon atmosphere of high purity (99.998%) at 825 °C with a growth rate of 1 mm/h. The source materials ^{7}LiF and YF_3 with the purity of 99.99% were produced in Russia and were taken with the ratio 52 mol % (lithium fluoride) and 48 mol % (yttrium fluoride). Lithium fluoride was of 99.7 at% purity of ^{7}Li. Erbium-166 isotope was added to the furnace of ^{7}LiYF$_4$ as oxide $^{166}Er_2O_3$ with the isotope concentration of 98% respectively. The single crystals were grown on a seed crystal with the orientation along the optical axis a. After the cleavage and polishing the sample has dimensions of 3×4×5 mm.

The sketch of experimental setup is shown in Fig. 1.

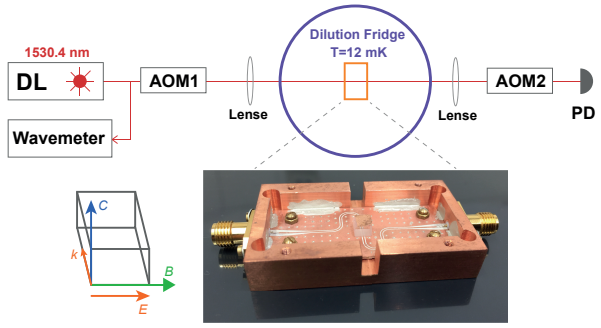

FIG. 1: (Color online) The experimental setup for studying of optical coherence. DL stands for the diode laser, PD is photoreceiver. Sample mount: the Er:LYF crystal is placed on the top of the microwave substrate. The orientation of the experiment is $B, E, k \perp c$, where c is crystal axis, E is polarization of the beam and k is the wave vector.

The crystal is placed on the top of microwave substrate Rogers TMM10i with 50 Ohm transmission line. The transmission line is intended for future experiments on frequency conversion and on long-lived spin quantum memory. In order to preserve good microwave properties of the setup no additional ultra-low temperature thermalization arrangements were implemented. The copper sample holder is mounted on the mixing chamber of cryogen-free BlueFors LD-250 dilution refrigerator. The magnetic field up to 0.3 T is created by the pair of superconducting Helmholtz coils and directed perpendicular to the c-axis of the crystal. The magnet is thermally anchored to the still stage of the dilution refrigerator and does not harm the performance of the dilution fridge. The field inhomogeneity was measured to be better than 10^{-4} in the sample volume. Our cryostat has an optical access in the horizontal direction which greatly simplifies optical experiments. Every radiation shield of the cryostat has two optical windows with gradually reducing diameter starting from 1.5 inch at room temperature down to 0.5 inch at the shield anchored to the cold plate (∼0.1 K). Optical windows are fabricated from Spectrosil 2000 material and AR-coated for the telecom-C wavelength range. The base temperature attainable for the developed cryogenic setup is 12 mK.

Transmission optical spectroscopy of $^4\mathrm{I}_{15/2} \leftrightarrow {}^4\mathrm{I}_{13/2}$ transition at $\lambda = 1530.37$ nm (vac) is measured by using a free-running single frequency tunable diode laser Toptica DL-PRO. The laser power is 40 mW and it has a linewidth of about 0.2 MHz during 1 sec of integration time. The laser frequency is constantly monitored at wavemeter HighFinesse WS6-600 and referenced across P_9 transition of fiber coupled $^{12}C_2H_2$ cell at $\lambda_{P9} = 1530.3711$ nm (vac). The laser field is focused with the f=30 cm lens into the crystal and the beam waist of ∼ 0.1 mm in diameter. The intensity of the transmitted signal is measured with an amplified InGaAs photoreceiver.

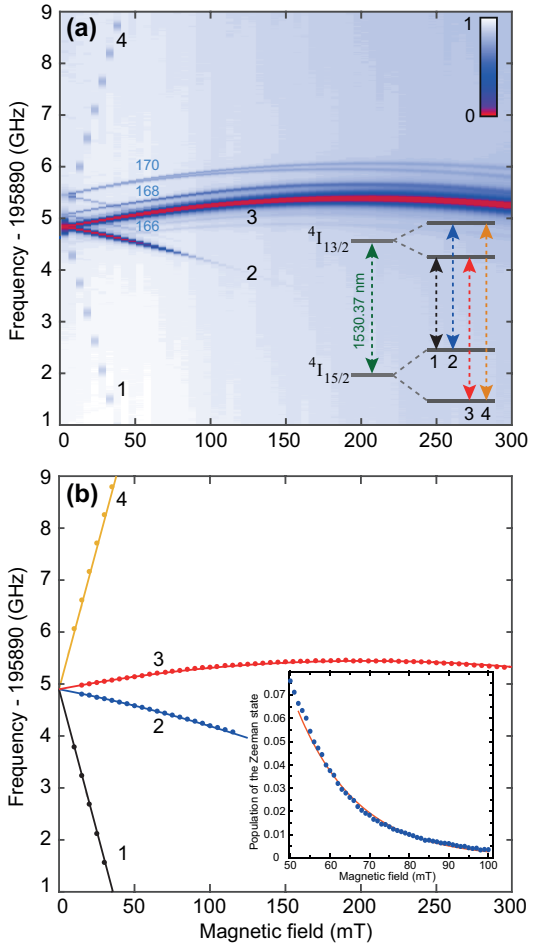

FIG. 2: (Color online) (a) Optical transmission spectrum of the Er:LYF crystal measured at the base temperature of the cryostat $T = 12$ mK as the function of the applied magnetic field. The color bar shows the magnitude of the transmitted signal. The frequency scans are taken in 5 mT steps. The level scheme of Er^{3+} ions in magnetic field shows the observed optical transitions. The weaker absorption signals are attributed to the traces of two additional isotopes ^{168}Er, ^{170}Er at ∼1 ppm concentration. (b) Dots corresponds to the measured transition frequencies of ^{166}Er determined from fits of individual absorption lines. Solid lines are the fit by using the Hamiltonian from [17]. (Inset) Population of the upper Zeeman state versus the magnetic field. Focused laser beam warms up erbium spin ensemble to some effective temperature T_{eff}. Solid line shows thermal depopulation of Zeeman state at $T_{\mathrm{eff}} = 90$ mK.

Figure 2(a) shows the measured transmission spectrum of our Er:LYF crystal as a function of the applied magnetic field. The excitation power of the laser field was set to 0.5 μW. Erbium ions are Kramers ions and they possess a half-integer spin. Every electronic state is split into two Zeeman levels if magnetic field is applied. Due to the high symmetry S_4 of the LYF crystal erbium ions substitute yttrium ions only in a single position and no

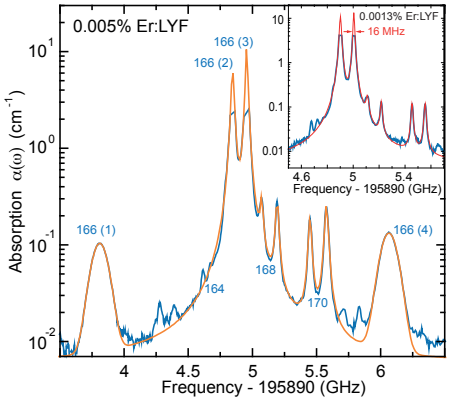

FIG. 3: (Color online) Absorption coefficient $\alpha(\omega)$ of the Er:LYF crystal extracted from the transmission spectrum at $B = 10$ mT. The inset shows the absorption coefficient of 0.0013% Er:LYF sample.

magnetic class splitting (as for Er:YSO) is present. The transmission spectrum consists of 4 lines: transitions 2 and 3 with small g-factor $g_{2,3} = 0.4$ and transitions 1 and 4 with larger one of $g_{1,4} = 7.7$. Because the Stark levels $I_{13/2}(0)$ and $I_{13/2}(1)$ of the optical excited state are only ~ 120 GHz apart [16] they mix at higher fields and result in dependence of g-factors on magnetic field. That mixing yields ZEFOZ point for the transition 3 at $B = 0.2$ T which is clearly visible on the spectrum.

The narrow optical inhomogeneous linewidth of our sample allowed us to resolve an isotopic shift. The weaker lines in the spectrum with the same field dependence are attributed to the traces of ^{168}Er and ^{170}Er isotopes at ~ 1 ppm residual concentration. The transition 3 for $^{170}Er^{3+}$ ion is found to split into two lines above 100 mT. This splitting is assumed to arise from the larger distortion of the crystal lattice by this specific isotope. Local distortions may led to the reduction of the local symmetry for erbium ions and appearing of non-equivalent magnetic positions (magnetic classes).

Transition 2 becomes more faint at higher fields due to thermal depopulation of the upper Zeeman sub-level of the optical ground state. Its population is extracted from the absorption coefficients $\alpha(\omega, B)$ and plot as the function of the applied magnetic field, see the inset in Fig. 2(b). The fit of the experimental data to Boltzman distribution yields an effective temperature of $T_{\rm eff} = 90$ mK for our erbium spin ensemble. This measurement shows the preparation of the spin ensemble in a single quantum state at weak magnetic fields, which is crucial for some quantum memory protocols.

The inhomogeneous broadening Γ of optical transitions is also extracted from $\alpha(\omega, B)$ at every recorded field point. Figure 3 displays the absorption coefficient measured at 10 mT. The absorption spectrum $\alpha(\omega, B)$ consists of many doublets corresponding to optical transitions between Zeeman levels of different isotopes. The orange line shows the fit of the total spectrum to the set of such contributions. Transitions 2, 3 are fit at best with Lorentzians, whereas transitions 1, 4 can be fit well with Gaussians. Full-width-half-maximum (FWHM) linewidth for transitions 2, 3 is $\Gamma_{2,3} = 35$ MHz and for transitions 1, 4 is $\Gamma_{1,4} = 130$ MHz. The linewidth of optical transitions is partially determined by super-hyperfine interactions with nuclei spins of the host crystal (mainly with fluorine) and reads as $\Gamma = \Gamma_0 + (g_e \pm g_g)\,\mu_B \delta B/\hbar + \delta g \mu_B B/\hbar$, where Γ_0 stands for the intrinsic linewidth due to the crystal strain, $g_{e,g}$ are g-factors of optical ground or excited states, δB is magnitude of very slow varying magnetic field created by the neighboring nuclei spins, sign + stands for transitions 1 and 4, sign − stands for transitions 2 and 3 [12, 13], and the term δg describes additional inhomogeneity of the crystal. Evaluation of the full data set for the measured linewidths yields intrinsic $\Gamma_0 = 23$ MHz and $\delta B = 1$ mT. We also note here, that FWHM linewidth as narrow as $\Gamma_{2,3} = 16$ MHz was observed with our sample doped with 0.0013% Er^{3+} ions, see inset in Fig. 3, which is in accordance with the record-narrow linewidth observed by R.M. Macfarlane et al. [1].

We study spin quantum dynamics of Er:LYF crystal by carrying out two- and three-pulse echo (2PE and 3PE) experiments. For that purpose, the laser field of 10 mW power level at the input of the cryostat was gated by a 200 MHz acousto-optical modulator in a single pass configuration. The typical length of the excitation pulses was ~ 1 μs. The emitted echo signal (~ 2 % efficiency) was picked up by the second acousto-optical modulator and detected by the amplified 200 MHz InGaAs photoreceiver. In order to avoid heating of the sample, the echo sequence was repeated with relatively slow rate of 1 Hz. At such rate no increase of the mixing chamber temperature was detected. The emitted signal was recorded on digitizing oscilloscope and averaged out by using PC. The averaged echo signal was fit at every delay time τ with $A{\cdot}\mathrm{sech}(t)$ function and the echo area A was extracted down to the 10^{-3} level. The echo decay was found to be non-exponential due to the presence of spectral diffusion. Therefore we used fit function suggested by W. Mims $I(\tau) = I_0 e^{-2(2\tau/T_M)^x}$, where T_M is phase memory time and x is the stretch factor [20].

The measured dependence of the phase memory time T_M and the stretch factor x on the applied magnetic field is plot in Fig. 4. The data are taken in a single experimental sequence during 24 hours of the total interrogation time. At zero field and $\tau > 3$ μs no echo was detected. Echo appears at fields above 10 mT. Due to the modulation of the echo signal, it was possible to reliably extract T_M and x only at field ranges $30 < B < 60$ mT and at $B > 150$ mT. Around 30-50 mT the phase memory time is nearly constant $T_M \simeq 10$ μs, which is very close to the value 12 μs observed at 1.5 K and high field [16, 19]. The stretch factor at weak fields is $x < 1$ and grows up

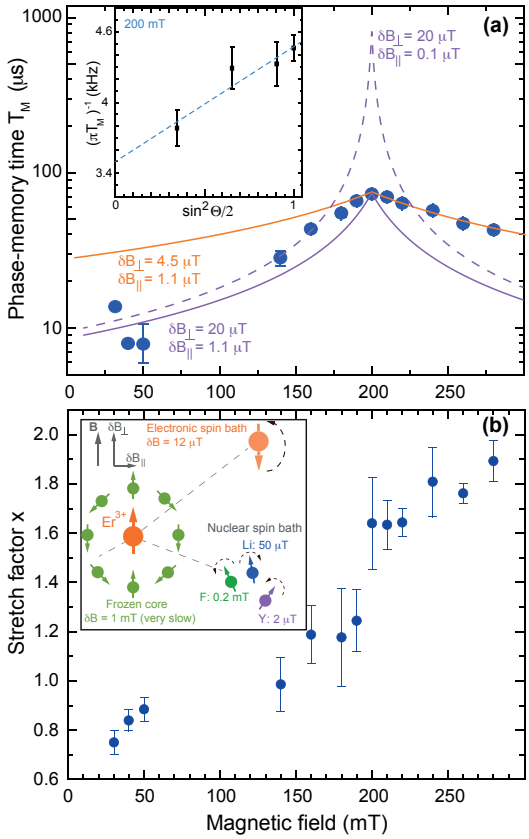

FIG. 4: (Color online) **(a)** Phase memory time T_M measured as the function of applied magnetic field by using 2PE sequence at the base temperature of the dilution refrigerator $T = 12$ mK. Filled circles are experimental data. Solid lines represent the behavior of T_M calculated for the different levels of the magnetic noise δB (see the text for details). Dashed line is the calculated T_M if $\delta B_\parallel = 0.1$ μT. The inset: evaluation of instantaneous optical diffusion. The line is the fit to the theory. **(b)** The stretch factor x measured as the function of the applied magnetic field. The inset: Magnetic noise contributions from different magnetic systems, i.e. "frozen core", electronic and nuclear spin baths. Orientation of magnetic noise components $\delta B_\perp$ and $\delta B_\parallel$ with the respect to the applied field B.

towards higher fields. Such behavior can be explained by slow spin-flip rates when electronic spin bath is polarized and the "frozen core" is formed, see ref. [21].

Around 200 mT the behavior of T_M shows a typical feature associated with ZEFOZ point. To our surprise, instead of showing of a rather sharp peak T_M was settled around 75 μs. In order to understand constrains on phase memory, we recall that its behavior around ZEFOZ point in the presence of magnetic noise $\delta\vec{B}$ is described by $T_M^{-1} = \vec{S_1}\cdot\delta\vec{B} + \hat{S}_2\cdot\delta\vec{B}\cdot\hat{S}_2 + (2T_1)^{-1}$, where $\vec{S_1}$ is the gradient and $\hat{S}_2$ is the curvature of the transition frequency with respect to the magnetic field [2, 6] and T_1 is optical relaxation time. In the case of Er:LYF crystal, $\vec{S_1}$ is zeroed in direction perpendicular to c-axis, but in other direction it is $S_1^\parallel = 11.95$ GHz/T. Therefore, the presence of magnetic noise along c-axis sets the upper bound for T_M on ZEFOZ. Solid lines in the Fig. 4 represent the calculated behavior T_M corresponding to magnetic fluctuations with magnitude of $\delta B_\perp = 4.5$ μT and 20 μT at $B_\parallel = 1.1$ μT. It is clearly seen that at ZEFOZ point T_M is determined by longitudinal magnetic noise $\delta B_\parallel$. At weak fields $B < 100$ mT the experimental data are closer to the curve calculated for the case of $\delta B_\perp \sim 20$ μT, whereas at higher fields it is better approximated with the curve corresponding to the more quiet magnetic environment with $\delta B_\perp \sim 4.5$ μT. The dashed line corresponds to the simulated $T_M(B)$ if the magnitude of longitudinal noise would be $\delta B_\parallel \sim 0.1$ μT.

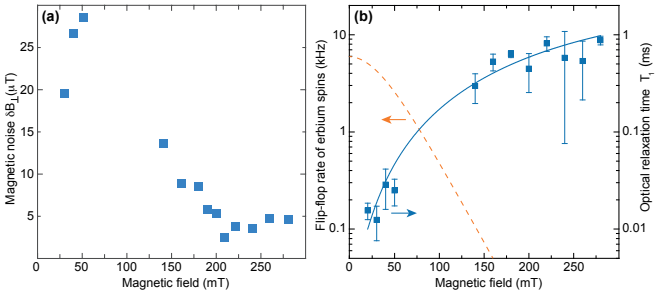

FIG. 5: (Color online) **(a)** Magnetic noise $\delta B_\perp$ calculated from $T_M(B)$ data. **(b)** Optical relaxation time T_1 measured in 3PE experiment as a function of the applied magnetic field at the base temperature of the cryostat 12 mK. Solid line is the fit describing contribution of erbium spins flip-flop. Dashed line is the calculated erbium spin flip-flop rate at $T_{\text{eff}} = 0.15$ K.

By evaluating T_M accordingly to our model we find the dependence of magnetic noise $\delta B_\perp$ on the applied field. The resulted data is shown in Fig.5(a). There are two primary decoherence sources: fluctuating electronic and nuclear spin baths. The magnitude of magnetic noise create by electronic spins can be estimated from $\delta B = \frac{\pi}{9\sqrt{3}}\mu_0 g_g \mu_B n_e \simeq 12$ μT, where $n_e \simeq 7\cdot 10^{17}$ cm^{-3} is concentration of erbium spins. At an effective temperature $T_{\text{eff}} \sim 0.15$ K erbium spin bath experiences significant polarization at $B \sim 100$ mT and erbium spin flip-flop rate is greatly reduced above this field value as shown in Fig.5(b), see also [9, 22]. In this field region the magnitude magnetic noise $\delta B_\perp$ rapidly drops from ~ 25 μT to ~ 4 μT. Electronic spin bath seems to partially contribute to the observed decoherence at low fields. Contribution from optical instantaneous diffusion was revealed by performing $\pi/2 - \tau - \Theta - \tau$−echo sequence. That yielded slightly higher value for $T_M = 91$ μs at ZEFOZ point, see the inset in Fig. 4(a).

Another contribution to the decoherence appears from nuclear spins. At our experimental conditions their Zeeman levels are nearly equally populated, hence the magnetic noise δB arising from nuclear spin flip-flops in a

bulk of the crystal (nuclear spin bath) is assumed to stay constant over the experimental field range. The magnitude of fluctuating fields contributed by F, Li and Y-ions are estimated to be 0.17 mT, 50 μT and 2 μT respectively. The estimated magnitude of magnetic noise created by nuclei spins of F and Li is higher than determined from the experimental data. That implies that the significant amount of F and Li nuclear spins flip at slower rates at higher fields and thus results in the reduced magnetic noise. We believe that the observed behavior of magnetic noise can be explained by using the concept of the "frozen core". Above 100 mT, polarized and quiet electronic spins freeze out nuclear spin flip-flop dynamics in their direct vicinity by detuning them from the rest of spin bath in a bulk of the crystal. The radius of the "frozen core" is estimated to be $r_0 = \sqrt[3]{\gamma_e/(2\gamma_n n_n)} \sim 3-8$ nm, where $\gamma_{e,n}$ are electronic and nuclei gyro-magnetic ratio and n_n is concentration of nuclear spins. This "frozen core" creates only a very slowly varying field of ~ 1 mT magnitude which broadens the optical line [13] but does not affect the phase relaxation. The further evidence of the development of the "frozen core" is also given by the observed non-exponential echo decay [2, 3].

The last contribution to the decoherence is due to the relaxation of optical dipoles and it was measured in 3PE experiment. The dependence of the T_1 on the applied magnetic field at the base temperature of the cryostat is shown in Fig. 5(b). The solid line displays the fit of the measured data to flip-flop process of erbium spins, see ref. [5]. The fit yields the effective temperature of the spin ensemble to be $T_{\text{eff}} = 0.15$ K.

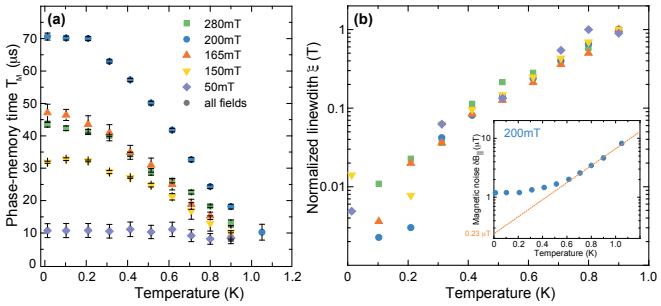

FIG. 6: (Color online) **(a)** Temperature dependence of the optical phase memory time T_M measured at the specific values of the magnetic fields. **(b)** Normalized linewidth ξ as the function of temperature. The inset: Magnetic noise $\delta B_{\|}$ calculated from $T_M(T)$ data measured at ZEFOZ field. Dashed line shows exponential behavior of $\delta B_{\|}$ at temperatures above 0.5 K.

In order to address an impact of the longitudinal magnetic noise on decoherence process we measured the temperature dependence of T_M, see Fig. 6(a). Above 1.5 K no echo was detected at pulse delay of $\tau = 3$ μs for all fields. Below 1 Kelvin, T_M grows up and saturates around 0.2 K for all magnetic fields, so does the stretch factor x. The longitudinal magnetic noise at ZEFOZ is calculated from $\delta B_{\|} = (T_M S_1^{\|})^{-1}$ and is plot as function of the temperature in the inset for Fig. 6(b). It decreases from 9 μT at 1 K to 1.1 μT below 0.4 K. We found that for all field values the dephasing rate T_M^{-1} is described by the same temperature dependence as $T_M^{-1} = a + b\xi(T)$, where a, b are constants which depend on magnetic field. But $\xi(T)$ is a function of temperature alone, its behavior is shown in Fig. 6(b). For the case of decoherence contribution from electronic spins we expect the T_M^{-1} would depend on B/T ratio, such as $\text{sech}^2(g\mu_B B/2k_b T)$ [5, 22]. Therefore, the magnetic noise $\delta B_{\|}$ is believed to arise from nuclear spin bath.

We admit that the deeper insight into the nuclear spin dynamics in the presence of polarizing electronic spins can be reached only with the developing of specific theoretical models. Quite advanced theoretical models have already been developed for donors in silicon, NV-centers in diamond and quantum dots [23–25]. For the case of RE-doped crystals only simple model was numerically studied [19]. More detailed theoretical investigation of spin dynamics of Er:YSO and Er:LYF crystals below 1 Kelvin will be done in the near future.

In conclusion, we demonstrated cw and time resolved optical spectroscopy of isotopically purified ^{166}Er:^{7}LYF$_4$ crystal below 1 Kelvin. Our fabricated crystals demonstrate record-narrow optical FWHM linewidths down to 16 MHz. We found that at sub-Kelvin temperatures spin coherence appears at weak magnetic fields and is limited by magnetic noise of electronic and nuclear spin baths. By presuming the similar decoherence mechanism for the ^{167}Er isotope we estimate hyperfine spin coherence time at ZEFOZ points to be $T_2^{hyp} \simeq 0.5$ ms. The presented experiment paves the way towards implementation of long lived off-Raman quantum memory by using narrow-linewidth solid state ensembles at sub-Kelvin temperature range. Also, such narrow-band atomic ensembles are very attractive for realization of quantum converters between telecom C-band optical photons and superconducting quantum circuits [26, 27]. In this respect, we have demonstrated storage/retrieval of coherent optical pulses at telecom C-band wavelength in erbium doped crystal at experimental conditions suitable for their operation.

We thank M. N. Popova, A. V. Masalov for stimulating discussions, P.B greatly acknowledges discussions with A. Tyryshkin and J. J. L. Morton. This work was supported by DFG through the grant INST 256/415-1 and the RSF grant No. 14-12-00806.

[1] W. Thiel, T. Böttger, and R. L. Cone, J. Lumin. **131**, 353 (2011).
[2] M. Zhong, M. P. Hedges, R. L. Ahlefeldt, J. G. Bartholomew, S. E. Beavan, S. M. Wittig, J. J. Longdell, and M. J. Sellars, Nature **517**, 177 (2015).

[3] M. Rancić, M. P. Hedges, R. L. Ahlefeldt, and M. S. Sellars, arxive **1611.04315** (2016).

[4] N. Sangouard, C. Simon, H. de Riedmatten, and N. Gisin, Rev. Mod. Phys. **83**, 33 (2011).

[5] T. Böttger, C. W. Thiel, Y. Sun, and R. L. Cone, Phys. Rev. B **73**, 075101 (2006).

[6] D. L. McAuslan, J. G. Bartholomew, M. J. Sellars, and J. J. Longdell, Phys. Rev. A **85**, 032339 (2012).

[7] S. R. Hastings-Simon, B. Lauritzen, M. U. Staudt, J. L. M. van Mechelen, C. Simon, H. de Riedmatten, M. Afzelius, and N. Gisin, Phys. Rev. B **78**, 085410 (2008).

[8] E. Baldit, K. Bencheikh, P. Monnier, S. Briaudeau, J. Levenson, V. Crozatier, I. Lorgeré, F. Bretenaker, J. Le Gouët, O. Guillot-Noël, et al., Phys. Rev. B **81**, 144303 (2010).

[9] S. Probst, H. Rotzinger, A. V. Ustinov, and P. A. Bushev, Phys. Rev. B **92**, 014421 (2015).

[10] S. Probst, H. Rotzinger, S. Wünsch, P. Jung, M. Jerger, M. Siegel, A. Ustinov, and P. A. Bushev, Phys. Rev. Lett. **110**, 157001 (2013).

[11] A. Tkalčec, S. Probst, D. Rieger, H. Rotzinger, S. Wünsch, N. Kukharchyk, A. D. Wieck, M. Siegel, A. V. Ustinov, and P. Bushev, Phys. Rev. B **90**, 075112 (2014).

[12] R. M. Macfarlane, A. Cassanho, and R. S. Meltzer, Phys. Rev. Lett. **69**, 542 (1992).

[13] R. M. Macfarlane, R. S. Meltzer, and B. Z. Malkin, Phys. Rev. B **58**, 5692 (1998).

[14] S. A. Moiseev and W. Tittel, New Journal of Physics **13**, 063035 (2011).

[15] X. Zhang, A. Kalachev, and O. Kocharovskaya, Phys. Rev. A **87**, 013811 (2013).

[16] R. Marino, I. Lorgeré, O. Guillot-Noël, H. Vezin, A. Toncelli, M. Tonelli, J.-L. L. Gouët, and P. Goldner, J. of Lumin. **169, Part B**, 478 (2016).

[17] K. I. Gerasimov, M. M. Minnegaliev, B. Z. Malkin, E. I. Baibekov, and S. A. Moiseev, Phys. Rev. B **94**, 054429 (2016).

[18] J. Ganem, Y. P. Wang, D. Boye, R. S. Meltzer, and W. M. Yen, Phys. Rev. Lett. **66**, 695 (1991).

[19] R. S. Meltzer, J. Ganem, Y. P. Wang, D. Boye, W. M. Yen, D. P. Landau, R. Wannemacher, and R. M. Macfarlane, J. Lumin. **53**, 1 (1993).

[20] W. B. Mims, Phys. Rev. **168**, 370 (1968).

[21] P. Hu and S. R. Hartmann, Phys. Rev. B **9**, 1 (1974).

[22] S. Takahashi, R. Hanson, J. van Tol, M. S. Sherwin, and D. D. Awschalom, Phys. Rev. Lett. **101**, 047601 (2008).

[23] W. M. Witzel, R. de Sousa, and S. Das Sarma, Phys. Rev. B **72**, 161306 (2005).

[24] W. M. Witzel, M. S. Carroll, L. Cywiński, and S. Das Sarma, Phys. Rev. B **86**, 035452 (2012).

[25] R. Guichard, S. J. Balian, G. Wolfowicz, P. A. Mortemousque, and T. S. Monteiro, Phys. Rev. B **91**, 214303 (2015).

[26] L. A. Williamson, Y.-H. Chen, and J. J. Longdell, Phys. Rev. Lett. **113**, 203601 (2014).

[27] S. Blum, C. O'Brien, N. Lauk, P. Bushev, M. Fleischhauer, and G. Morigi, Phys. Rev. A **91**, 033834 (2015).